Numerical Simulation of Particle Breakage in Dry Impact Pulverizer

Hirohisa Takeuchi, Hideya Nakamura, and Satoru Watano
Dept. of Chemical Engineering, Osaka Prefecture University, Sakai, Osaka 599–8531, Japan

DOI 10.1002/aic.14096
Published online April 2, 2013 in Wiley Online Library (wileyonlinelibrary.com)

A novel method to simultaneously simulate particle motion and its breakage in a dry impact pulverizer was developed. The motion of particles in the pulverizer was calculated using a discrete phase model (DPM)-computational fluid dynamics (CFD) coupling model. When the particle impacts against a vessel wall, impact stress acting on the particle is calculated from Hertz's theory as a function of the impact velocity. At the same time, the particle strength as a function of the particle size is calculated from Griffith's theory. If the impact stress is larger than the particle strength, the particle is broken and replaced with smaller fragments. The size distribution of the fragments is obtained from a breakage function proposed. The motion of the fragments is calculated again by using the DPM-CFD coupling model. By repeating the above calculations over the whole particles, the grinding phenomenon can be simulated. The calculated results showed good agreement with the experimental one, and validity of the proposed method was confirmed. © 2013 American Institute of Chemical Engineers *AIChE J*, 59: 3601–3611, 2013
Keywords: simulation, process, particle technology, multiscale modeling

Introduction

A dry-grinding process is widely used for size reduction of particulate materials. The size distribution of the ground products influences very much on the quality and performance of the end products. For example, in the pharmaceutical industries, the size distribution of ground active pharmaceutical ingredients (APIs) and excipients can drastically affect dissolution rate and solubility of the APIs. This implies the accurate control of size distribution of the ground products is significantly important.

To produce the ground products having desired size distribution, a dry-grinding process should be designed and controlled with understanding of the particle-grinding phenomenon in the grinding process. So far, the particle-grinding phenomenon has still not been understood due to its complexity. Thus, the process design and optimization of the operating conditions have been well-conducted by a trial-and-error approach based on the experience of experts. Therefore, the particle-grinding phenomenon in the dry-grinding process should be fully understood.

To understand the particle-grinding phenomena in a dry-grinding process, two main phenomena should be understood. The first phenomenon is how the particles move in the grinding equipment and how much impact stress the particles receive when the particles impact against the vessel wall or other particles. The second one is how the particles are broken and split into the smaller particles, namely fragments, after the particles received the impact stress. To analyze these two phenomena simultaneously, numerical simulations should be used. The motion of particles, fluid, and grinding media in grinding equipment has been well-analyzed[1–11] using a discrete element method (DEM), computational fluid dynamics (CFD), and DEM-CFD coupling model. The motions of particles, fluid, and grinding media in many grinding devices have been successfully simulated, and an energy, velocity, and frequency of particle impacts have been well-characterized as a function of the operating parameters. However, these simulation methods cannot treat the particle breakage phenomena. On the other hand, the particle breakage phenomena have been analyzed using a finite element method,[12] agglomerated DEM particle,[13] and population balance model.[14] It is reported that a fragment-size distribution after a single-particle breakage strongly depends on the impact velocity,[12–14] impact angle,[13] and material properties.[14] For example, Kalman et al.[15] conducted modeling of a single-particle breakage into fragments after the particle impact against the wall. However, these studies analyzed only a single-particle breakage and did not consider the whole particle breakage in a grinding process. In summary, although many numerical simulations of grinding process have been proposed and the single-particle breakage have been reported, only a few studies have reported that particle motion and its breakage in a grinding process are analyzed simultaneously.

A few methods[16–20] have been proposed for the coupling of particle motion and its breakage in a grinding process. In these methods, the motion of particles was calculated using a DEM. In terms of a concept of modeling of the particle breakage, the simulation methods can be categorized into the two approaches, that is, an agglomerated particle model[21,22]

Correspondence concerning this article should be addressed to H. Nakamura at hnakamura@chemeng.osakafu-u.ac.jp.

and a fragmentable particle model.[19,20] In the agglomerated particle model, individual particles are treated as an agglomerate, which consists of many small elements. In the fragmentable particle model, individual particles are split into small fragments based on a probability distribution function, that is, a breakage function, when the particle is broken. Herbst et al.[16,17] and Lichter et al.[18] used the agglomerated particle model for simulations of the particle breakage in grinding processes. However, the calculated particle-size distribution of the ground particles did not show good agreement with the experimental ones,[16–18] especially, within the range of fine particle size. This indicates that the agglomerated particle model has a disadvantage regarding generation of fine fragments after the particle breakage, because the single particle in the agglomerated particle model consists of small elements bonded each other, leading that the minimum size of the fragments is needed to be determined in advance. In addition, the agglomerated particle model has a disadvantage regarding its computational cost, because huge numbers of bonds connecting the small elements are required. On the other hand, the fragmentable particle model can simulate fine particles more accurately than the agglomerated particle model with lower computing cost, because the minimum size of the fragments can be determined based on the impact conditions such as the impact velocity and particle size. Cleary et al.[19] simulated particle breakage in a simple rotating two-dimensional box using a fragmentable particle model. He described the particle breakage by replacing a mother particle with some smaller fragments. However, mass of the particle before and after the particle breakage was not conserved. Bruchmüller et al.[20] attempted to use a fragmentable particle model to simulate particle breakage in a tumbling ball mill. However, the particle breakage could not be successfully simulated, because the particle strength was not estimated properly. Therefore, no simulation method which can analyze particle motion and its breakage simultaneously in a grinding process has been yet established.

In this study, a novel method to simulate the particle motion and its breakage simultaneously in a dry impact pulverizer has been proposed. First, a new particle breakage model which was based on the fragmentable particle model was proposed. In the particle breakage model, particle strength and impact stress acting on the particles were calculated based on Griffith's theory and Hertz's theory. Sizes of the fragments after the particle breakage were calculated from a breakage function. Parameters used for calculating the particle strength and size distribution of the fragments were obtained from a uniaxial compression test and impact breakage test. The fluid and particle motion in a grinding process was simulated by a discrete phase model (DPM)-CFD coupling model. Then, the proposed particle breakage model was coupled with the numerical simulation of fluid and particle motion in a dry impact pulverizer. By using the developed simulation method, a temporal change in particle-size distribution was simulated. Location of the particle breakage in the grinding chamber and particle size before the particle breakage were also analyzed. Finally, the calculated particle-size distribution after the grinding was compared with the experimental one.

Particle Breakage Model

Overview of the particle breakage model

In this study, the particle breakage in a grinding process was described by three components; the particle strength, the impact stress acting on the particle, and the fragment-size distribution after the particle breakage.

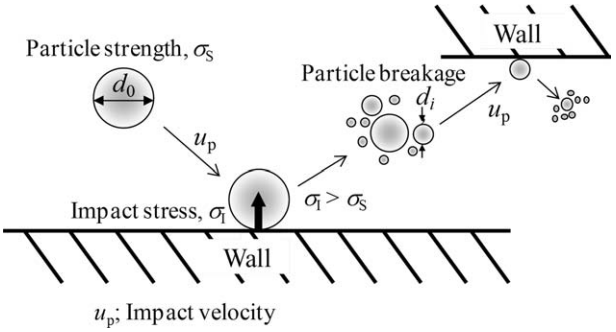

Figure 1. Schematic of particle breakage model.

Figure 1 shows a schematic of a particle breakage model proposed. When a particle impacts against a wall at an impact velocity u_p, the particle receives an impact stress σ_I. If the impact stress σ_I is higher than the particle strength σ_S ($\sigma_I > \sigma_S$), the particle is broken. The particle then splits into multiple smaller fragments having different sizes of d_i ($i = 1, 2, 3, \cdots$). The breakage process will be repeated in the grinding chamber. In the following, proposed three components are explained in detail.

Particle strength

The particle strength is defined by Griffith's theory. The particle strength is calculated by the following equation[23]

$$\sigma_s = \left(\frac{2\gamma E}{\pi C}\right)^{0.5} \tag{1}$$

where γ and C express a surface energy per unit area and half-length of a crack which is an onset of a particle breakage, respectively. The particle strength has a distribution even if the size and properties are the same, because the crack length is not uniform and has its distribution. In our preliminary investigation, it was found that the particle strengths measured experimentally can be well-expressed by Griffith's theory under an assumption that distribution of the crack length obeys a log-normal distribution. Therefore, the crack length C was decided to be described by a following log-normal distribution

$$f(C) = \frac{1}{\sqrt{2\pi}C\ln S_c}\exp\left[-\frac{1}{2}\left(\frac{\ln C - \ln \mu_c}{\ln S_c}\right)^2\right] \tag{2}$$

where S_c and μ_c indicate geometric mean and standard deviation of the crack length, respectively.

Impact stress

When an elastic spherical particle impacts against a wall at the impact velocity u_p, maximum load acting on the particle can be calculated by the following equation[24] derived from Hertz's theory

$$F_I = \left(\frac{5\rho_p \pi}{3}\right)^{0.6}\left(\frac{4}{3k}\right)^{0.4}\left(\frac{d_0}{2}\right)^2 u_p{}^{1.2} \tag{3}$$

where ρ_p and d describe particle density and particle diameter, respectively. k is the material mechanical property which is defined by the following equation

$$k = \frac{1-{v_1}^2}{E_1} + \frac{1-{v_2}^2}{E_2} \tag{4}$$

where E and v are the Young's modulus and Poisson's ratio, respectively. The subscripts of 1 and 2 mean the wall and particle, respectively. By dividing Eq. 3 by the particle projected area, the impact stress acting on the particle can be described as follows

$$\sigma_I = \left(\frac{5\rho_p}{3}\right)^{0.6} \left(\frac{4}{3k}\right)^{0.4} {u_p}^{1.2} \tag{5}$$

Fragment-size distribution after particle breakage

The fragment-size distribution after the particle breakage can be described by a breakage function.[25,26] In this study, a power-law function, which is a common breakage function,[27,28] was used

$$B = \left(\frac{d_i}{d_0}\right)^a \tag{6}$$

where d_i and d_0 ($d_i < d_0$) are the particle diameter of a fragment and a particle diameter before the breakage, respectively. a is a parameter which determines width of the fragment-size distribution. B means volume ratio of fragments smaller than d_i in the all fragments.

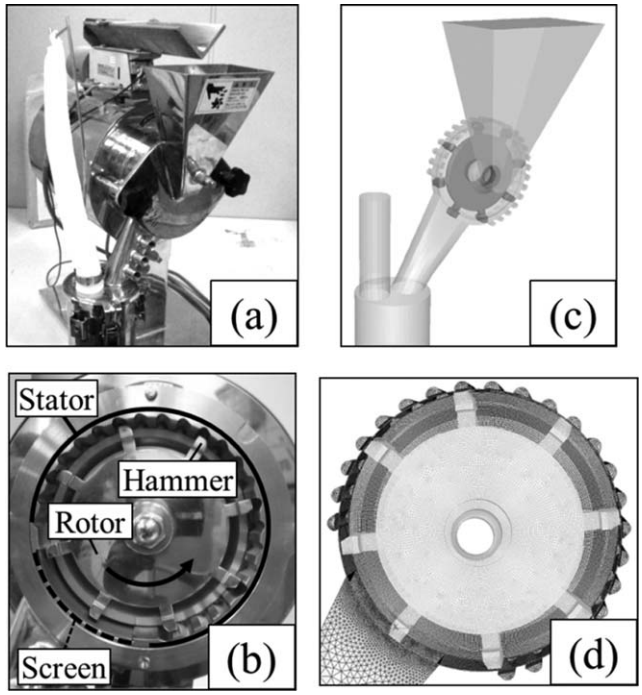

Figure 2. Pictures of dry impact pulverizer.

(a) Overview, (b) grinding chamber, (c) simulated geometry of grinding equipment, and (d) simulated geometry of grinding chamber.

Numerical Simulation of Fluid and Particle Motion in Dry Impact Pulverizer

Grinding process

An impact pulverizer (LM-05, Fuji Paudal Co.) was used in this study.[8] An actual appearance and grinding chamber of the pulverizer are shown in Figures 2a, b. The impact pulverizer consists of a high-speed rotating rotor having eight hammers with dimensions of 15 mm in width, 8 mm in height, and 8 mm in depth, a grinding chamber with a diameter of 119 mm and a depth of 30 mm, a concavo-convex-shaped stator on the chamber wall, a classification screen with opening size of 0.7 mm in diameter, and a collection pot of a final ground product. A minimum gap between the hammer tip and the stator protuberance is 0.5 mm. An original particulate material is continuously fed into the center of the chamber and ground between the high-speed rotating hammer and the static stator. The ground particles which pass through the classification screen are collected in the collection pot as a final ground product.

Numerical simulation of fluid flow and particle motion

The fluid flow and particle motion in the impact pulverizer were simulated[8] using a DPM-CFD coupling model. Simulated geometries of the whole grinding process and the grinding chamber are indicated in Figures 2c, d. The fluid flow in the impact pulverizer is extremely high-speed turbulent flow caused by the high-speed rotating hammers. Thus, the fluid was assumed to be a viscous and compressible fluid, and the fluid flow was considered as a turbulence and unsteady flow in the CFD simulation. Effect of the turbulence was described by a Reynolds averaging procedure.[29] As a turbulence model, a modified k-ε model[30] was used because it can simulate a swirling turbulent flow accurately. The motion of the individual particles was calculated using the DPM. In the DPM, the particles were treated as point masses, and the particle-to-particle impacts were not taken into account because the particle concentration in the impact pulverizer was low.[8] For the coupling between DPM and CFD, a one-way coupling model was used. In the one-way coupling model, the effect of the fluid motion on the particle motion was only considered, whereas effect of the particle motion on the fluid motion was not considered. The individual particle motion was calculated by solving the equation of particle motion as follows[8]

$$m_p \frac{d\boldsymbol{u}_p}{dt} = \boldsymbol{F}_d + m_p \boldsymbol{g} - m_p \boldsymbol{g} \frac{\rho_f}{\rho_p} \tag{7}$$

$$\boldsymbol{F}_d = C_d \frac{\pi {d_p}^2 \rho_f}{8} |\boldsymbol{u} - \boldsymbol{u}_p| (\boldsymbol{u} - \boldsymbol{u}_p) \tag{8}$$

where m_p, $\boldsymbol{F}_d$, $\boldsymbol{g}$, and ρ_f are particle mass, fluid drag force, gravity acceleration, and fluid density, respectively. $\boldsymbol{u}$ is the fluid velocity simulated by the CFD. The coefficient of fluid drag C_d is obtained from an empirical correlation.[31] The coefficient is written as follows

$$C_d = \frac{K_1}{Re_p} + \frac{K_2}{Re_p^2} + K_3 \tag{9}$$

$$Re_p = \frac{\rho_f d_p |\boldsymbol{u}_p - \boldsymbol{u}|}{\mu} \tag{10}$$

where Re_p and μ are particle Reynolds number and fluid viscosity, respectively. K_1, K_2, and K_3 are empirical constants,[31] which are determined depending on Re_p. Eq. 9 can be applied in a wide range of Re_p ($Re_p < 5.0 \times 10^4$).

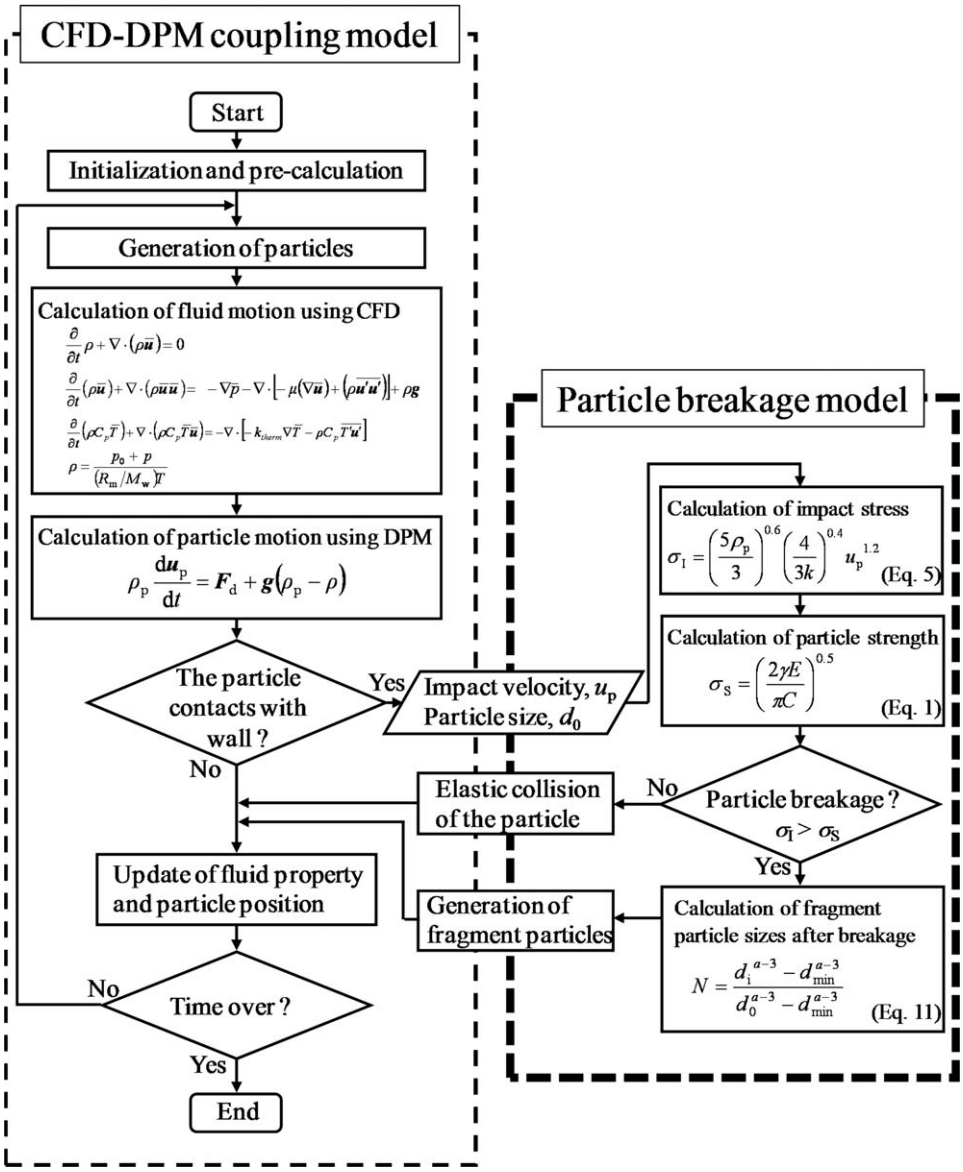

Figure 3. Flow chart of proposed simulation method.

Implementation of Particle Breakage Model into CFD-DPM Coupling Model

Figure 3 shows a flow chart of the proposed simulation method. First, the fluid flow and particle motion in the impact pulverizer were calculated using the DPM-CFD coupling model. When a particle impacts against a wall of the grinding chamber, the impact stress acting on the particle (σ_I) was calculated from Eq. 5 using the particle impact velocity (u_p). The particle strength (σ_S) was then determined. To calculate the particle strength (σ_S), two parameters μ_c and S_c in Eq. 2 were initially calculated from diameter of the impacted particle (d_0). A crack length C of the impacted particle was then calculated based on the Eq. 2 with the calculated μ_c and S_c. In the numerical simulation scheme, the crack length C was determined from generated random numbers obeying the log-normal distribution of the Eq. 2. A Box–Muller transform method[32] was used to generate the random numbers. This transform method can calculate random numbers obeying normal distribution functions from uniform random numbers. The uniform random numbers were calculated using a Mersenne Twister algorithm.[33] By substituting the crack length C into Eq. 1, the particle strength (σ_S) was finally determined. The mechanical properties of the wall and particle in Eqs. 4 and 5 are shown in Table 1. If the impact stress is smaller than the particle strength ($\sigma_I \leq \sigma_S$), the particle is not broken and rebounds from the wall as an elastic collision. The restitution coefficient was 0.95.[34] On the other hand, if the impact stress is larger than the particle strength ($\sigma_I > \sigma_S$), the particle is

Table 1. Material Properties

Property	Particle (Glass Beads)	Wall (SUS-304)
Young's modulus E (GPa)	71	200
Poisson's ratio ν (—)	0.25	0.25
Density ρ (kg/m^3)	2500	
Surface energy γ (J/m^2)	4.1	

Table 2. Calculation Conditions

Fluid viscosity (Pa s)	1.789×10^{-5}
Inlet pressure (Pa)	101,325
Outlet pressure (Pa)	101,325
Rotor rotating speed (rps)	267
Time step (s)	8.33×10^{-6}
Original particle diameter (μm)	500
Particle density (kg/m^3)	2500
Restitution coefficient (—)	0.95

broken and splits into fragments. The sizes of the fragments are calculated based on the breakage function shown in Eq. 6. The parameter a in Eq. 6 was calculated as a function of the particle impact velocity. The correlation between the parameter a and the particle impact velocity was obtained from the experimental results of an impact breakage test. To calculate the sizes of the fragment particles, the breakage function should be converted from a volume basis to a number basis. The number-based breakage function N converted from Eq. 6 is shown as follows[15]

$$N = \frac{{d_i}^{a-3} - d_{\min}^{a-3}}{d_0^{a-3} - d_{\min}^{a-3}} \tag{11}$$

where d_0 and $d_{\min}$ are the particle diameter before breakage and the minimum diameter of the fragments, respectively. In this study, $d_{\min}$ was defined as the d_i at $B = 0.01$ in Eq. 6 to achieve both better accuracy of calculated fragment size and lower computing cost, although a particle smaller than $d_{\min}$ might be generated in an actual particle breakage. The sizes of the individual fragments d_i ($i = 1, 2, 3, \ldots$) were calculated one-by-one from Eq. 11. The maximum total number of the fragments after the single-particle breakage was set as 30. This maximum number of the fragments was also preliminary optimized to achieve both better accuracy of calculated fragment size and lower computing cost. The individual fragments were generated until whether the total volume of the fragments reached to the 98 vol % of the impacted original particle, or the total number of the fragments reached to 29. Only one fragment was then finally generated, and its size was determined to conserve the mass balance before and after the particle breakage. According to this simulation procedure, the particle motion and its breakage in the grinding process can be simulated simultaneously.

Calculation conditions

The numerical simulation was performed using the Fluent software (v12.0, ANSYS). The proposed particle breakage model was implemented into the software using a user define function. The calculation conditions are listed in Table 2.

After a converged (quasisteady) fluid flow was simulated without particles, a single particle was fed into the center of the grinding chamber every 8.33×10^{-6} s. As a model particle used in the calculation, glass beads that have a diameter of 500 μm were used. The rotating speed was 267 rps. All computations were performed using a work station (VT64 WorkStation9500, Intel Xeon X5690 3.46 GHz, Visual Technology). It took about 36 h to calculate the converged fluid flow without the particles and 10 days to simulate the fluid motion, particle motion, and its breakage for 15 ms.

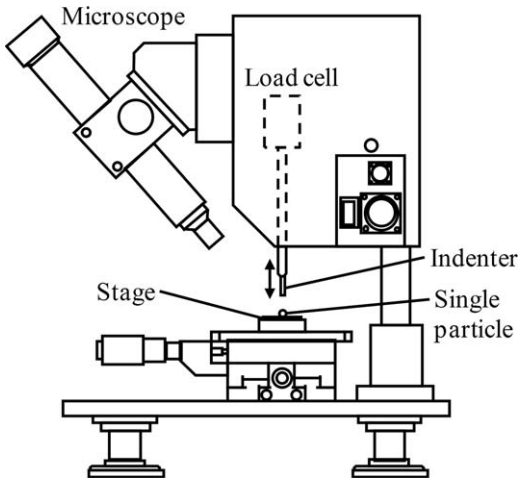

Figure 4. Schematic of particle hardness tester.

Experimental

Model particle

Lime soda glass beads (Toshin Rikou Co.) with spherical shape and a typical brittle property were used as a model particulate material. The material properties are shown in Table 1.

Uniaxial compression test

To obtain the parameters S_c and μ_c in the crack-length distribution (Eq. 2), single-particle strengths were measured by a particle strength tester (Grano 3.01, Okada Seiko Co.). Figure 4 shows a schematic of the tester. A single particle is broken by compression with the indenter. The tester can measure the compression load and the displacement of the indenter when a particle is broken. The moving velocity of the indenter was set as 100 μm/s. The particle strength was calculated by dividing the maximum compression load F_B by the projected area of the particle when the particle was broken

$$\sigma_s = \frac{F_B}{\pi d^2/4} \tag{12}$$

The original particles were sieved into size ranges of 106–125, 180–212, 180–212, 425–500, and 650–710 μm. The particle strengths of 100 particles within each size range were measured.

Impact breakage test

Impact breakage test was conducted to obtain the parameter a in Eq. 6. In this test, fragment-size distribution after the particle breakage was measured. Figure 5 shows a schematic of the experimental apparatus. The apparatus consists of a high-speed rotor ($\phi = 119$ mm) covered with a box, pneumatic conveying unit, and a bag filter to collect particles after impact against the tip of the rotor. The original particles were transported to a tip of the rotor, and the particles were impacted against the tip only once. The impact velocity can be changed up to 100 m/s by adjusting the rotating speed of the rotor. When the particles impacted against the rotor, the direction of the particle motion is changed, and the particles are collected to the bag filter. Thus, this

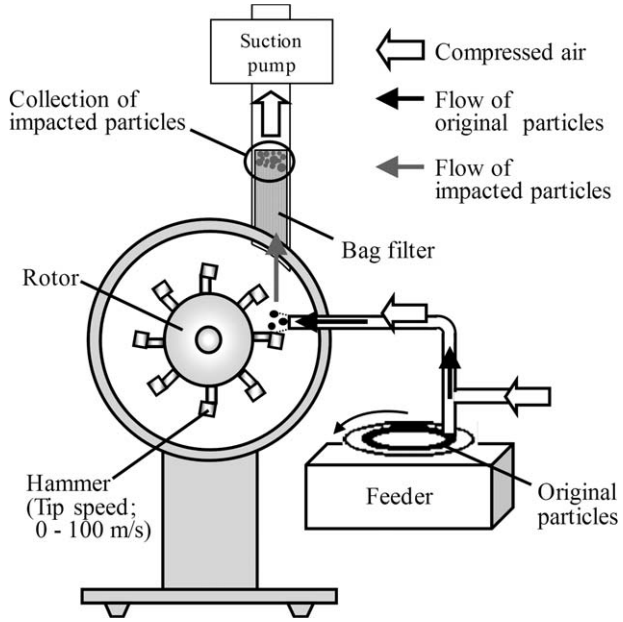

Figure 5. Experimental set-up of impact breakage test.

experimental apparatus can collect only particles impacted against the rotor. The original particles used in this test were the glass beads shown in Table 1 and sieved into a size range of 425–500 μm. The size distribution of the collected particles was measured by a sieve analysis.

Grinding by impact pulverizer

To compare the calculated result of the particle-size distribution of a final ground product with the experimental one, a grinding experiment was conducted using the impact pulverizer. The experimental conditions were the same as the simulation condition. Size and geometry of the impact pulverizer and diameter and density of the particle used in the experiment were also the same with those in the numerical simulation. The particle-size distribution of the final ground product was measured by a sieve analysis.

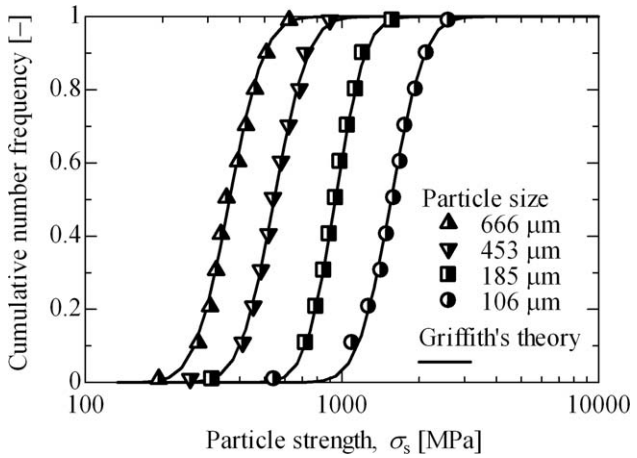

Figure 6. Particle-strength distribution under various particle sizes.

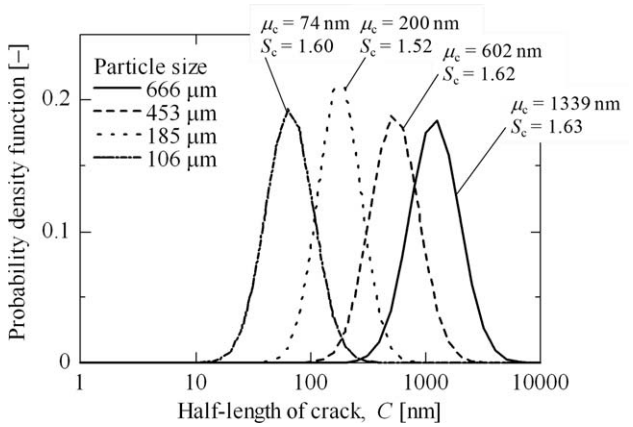

Figure 7. Calculated crack-length distributions under various particle sizes.

Results and Discussion

Effect of particle size on particle-strength distribution

Figure 6 shows a cumulative number frequency of particle strength under various particle sizes. Even when the size and the material properties of the original particles were the same, the particle strength was distributed. This was because that length of a crack which was an onset of a particle breakage has a distribution. With a decrease in the size of the particle, the particle strength was increased. Red lines in Figure 6 show the fitting results by the Griffith's theory under the assumption that the crack length has a log-normal distribution, as shown in Eqs. 1 and 2. It was found that the equations well-described the experimental results of the particle strength under various particle sizes. Figure 7 shows crack-length distributions under various particle sizes, calculated by Eq. 2. With a decrease in the particle size, the calculated crack length was decreased. This result well-explained the reason why the smaller particles showed higher strength, as shown in Figure 6. Width of the crack-length distribution was almost constant regardless of the particle size. Figure 8 shows correlations of the parameters S_c and μ_c in Eq. 2 with the particle diameter d. It was found that the geometric mean of the crack length (μ_c) strongly depended on the particle size, whereas the standard deviation of the crack length S_c was almost constant. From these correlations, empirical equations of the parameters S_c and μ_c as a function of particle diameter d were proposed

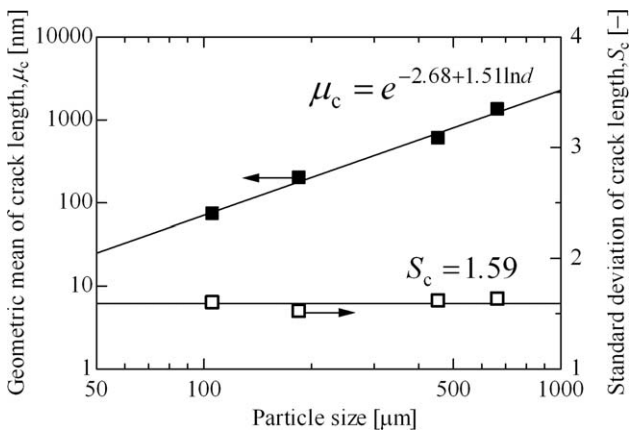

Figure 8. Correlation between parameters of crack-length distribution and particle size.

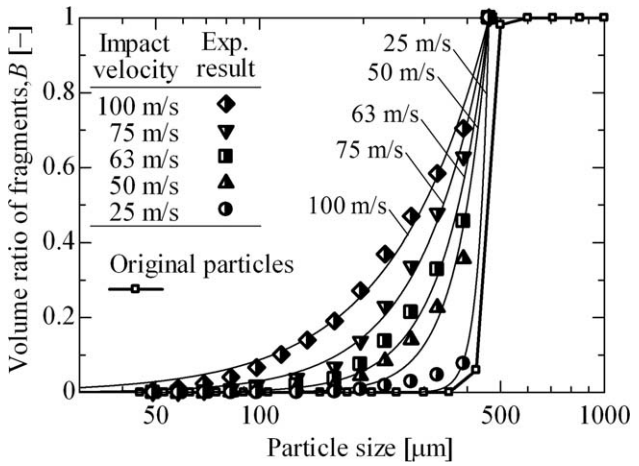

Figure 9. Fragment-size distribution under various impact velocities.

$$\mu_c = e^{-2.68+1.51\ln d} \tag{13}$$

$$S_c = 1.59 \tag{14}$$

By using Eqs. 13 and 14, the particle strength at any size of the particle can be calculated.

Effect of impact velocity on fragment-size distribution

Figure 9 shows mass-based fragment-size distributions under various impact velocities. At the lowest impact velocity (25 m/s), more than 90% of the fragment particles were coarse fragments larger than 400 μm. This result indicated that the particles were mainly broken by attrition. However, with an increase in the impact velocity, frequency of the coarse fragment particles was decreased. This result showed the particles were mainly broken by volume grinding at the higher impact velocity. This was because that at the higher impact velocity the crack could widely propagate and reach to inside of the particle.[35] Therefore, it was found that the fragment-size distribution strongly depended on the impact velocity and should be modeled as a function of the impact velocity. The lines in Figure 9 indicate the fitting results by the breakage function shown in Eq. 6. The fitting results well-described the experimental results at the higher impact velocities, although the fitting results were slightly different to the experimental results at the lower impact velocities. This was because that the breakage function used here could describe size distribution of finer fragments accurately rather than coarser fragments.[27] Nevertheless, the breakage function can well-describe the experimental results in the range of the impact velocities within 25 and 100 m/s. Thus, the breakage function shown in Eq. 6 was found to be used to calculate the fragment-size distribution after a particle breakage.

Figure 10 shows a correlation of the parameter a in Eq. 6 with the impact velocity of the particle u_p. With an increase in the impact velocity, the parameter a was decreased. This meant that width of the fragment-size distribution became wider with an increase in the impact velocity. The parameter a strongly depended on the impact velocity u_p. Finally, an empirical equation of the correlation between the a and u_p was obtained

$$a = 2684 u_p^{-1.625} \tag{15}$$

Through this equation, a breakage function could be determined as a function of the impact velocity.

Simulation results of particle breakage in an impact pulverizer

The proposed particle breakage model, which can calculate the particle strength, the impact stress acting on the particle, and the fragment-size distribution after the particle breakage, was implemented into the DPM-CFD coupling model to simulate the motion and the breakage of whole particles in the impact pulverizer. Figure 11 shows snapshots of particle distribution in the grinding chamber at different grinding times. $t = 0$ ms means the starting time of the particle breakage. The particles are colored according to its particle size, and the size of the particle is enlarged by two times to clearly visualize. The particles were initially transported from center to circumference of the grinding chamber. With an increase in the grinding time, the particles were broken and many fragments were generated, resulting in a drastic increase in number of the particles. The total number of the particles reached to about 3,340,000 at $t = 15.0$ ms, which was more than 1700 times as much as the original particles (500 μm) which were fed into the grinding chamber.

Figure 12 shows temporal change in the number-based particle-size distribution in the grinding chamber. Figure 13 shows the number-based particle median diameter as a function of the grinding time. At an early stage of the grinding operation, the grinding rate was very high. Even for a short grinding time ($t = 1.7$ ms), the particle-size distribution quickly shifted to a smaller particle size and the particle median diameter decreased to less than one-fiftieth of the original particle size. At the early stage of the grinding, the strength of the most of the particles was much smaller than the impact stress. Thus, the most of the particles impacting against the wall could be broken. After $t = 6$ ms, however, the particle-size distribution was almost unchanged. This was because that the particle strength increased with a decrease in the particle size. In addition, the impact stress was decreased with a decrease in the particle size.[7] This leads to difficulties of the particle breakage. The calculated temporal change showed similar propensity with an actual grinding phenomena, namely, a grinding limit.

Analysis of particle breakage in grinding chamber

Figure 14 shows number-based size distributions of the particles just before the particle breakage, shown as d_0 in Figure 1, in the grinding chamber. The size of the particles

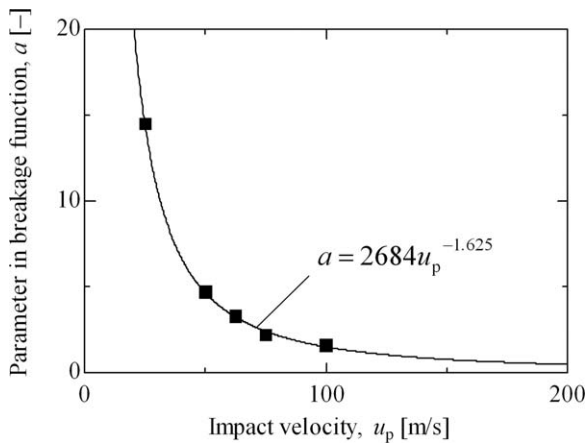

Figure 10. Correlation between parameter *a* in breakage function and impact velocity.

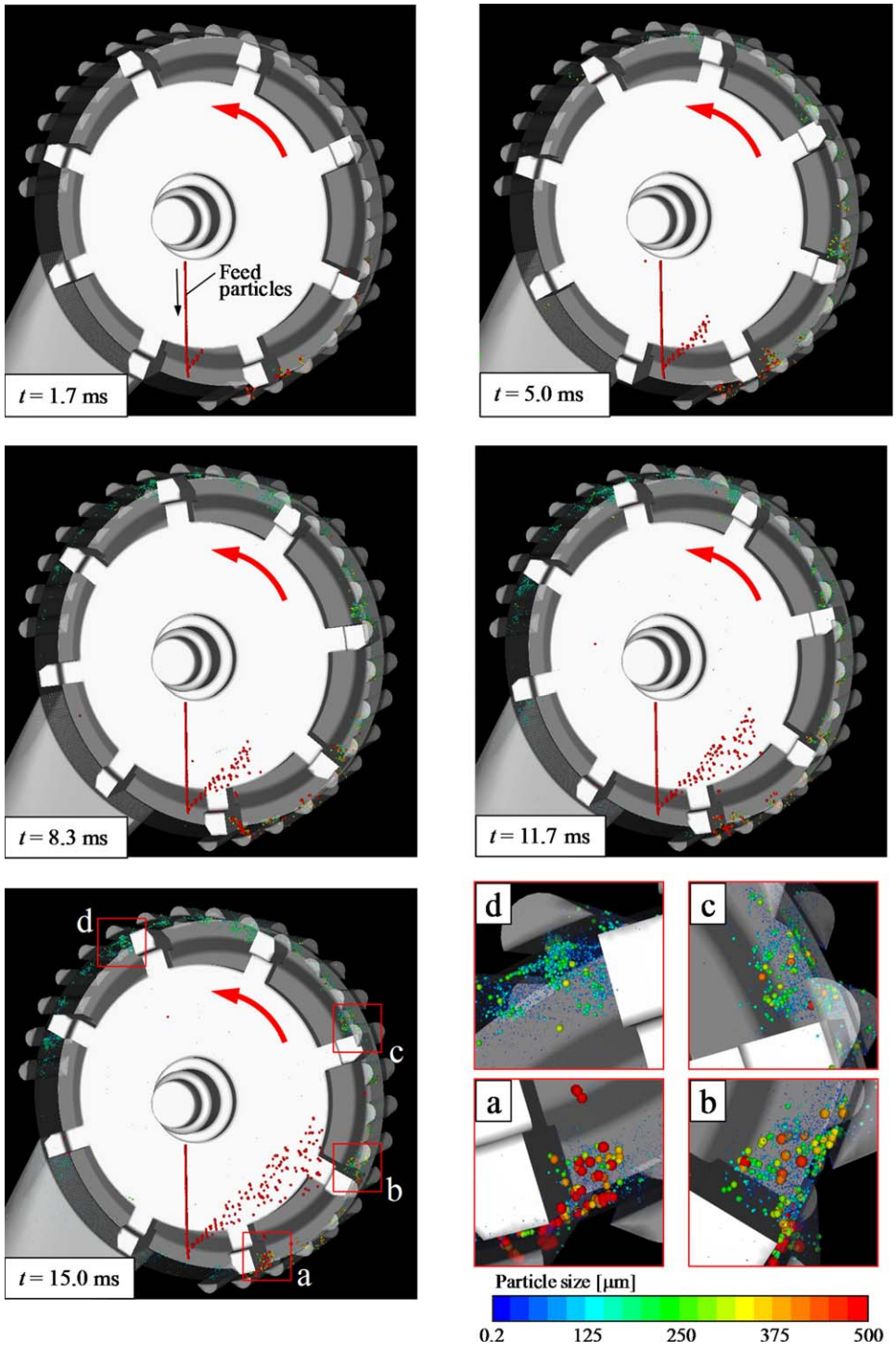

Figure 11. Particle distribution in grinding chamber.

[Color figure can be viewed in the online issue, which is available at wileyonlinelibrary.com.]

was decreased with an increase in the grinding time. However, the size of d_0 did not show smaller than 40 μm. This size limitation was determined from relation between an attainable maximum impact stress acting on the particle and its particle strength. The attainable maximum impact stress was determined from the type of the grinding equipment and the operation conditions. Therefore, the particles smaller than about 40 μm were not broken, because the attainable maximum impact stress derived from intrinsic performance of the impact pulverizer could not exceed the strength of the particles smaller than 40 μm particle. Accordingly, the size limitation of the particles which can be broken was well-expressed in the proposed simulation method.

Comparison with experimental results

The particles in the grinding chamber are discharged thorough the classification screen and collected in the collection pot as a final ground product. Figure 15 indicates a temporal change in calculated particle-size distribution of the final ground product collected in the collection pot. In an early

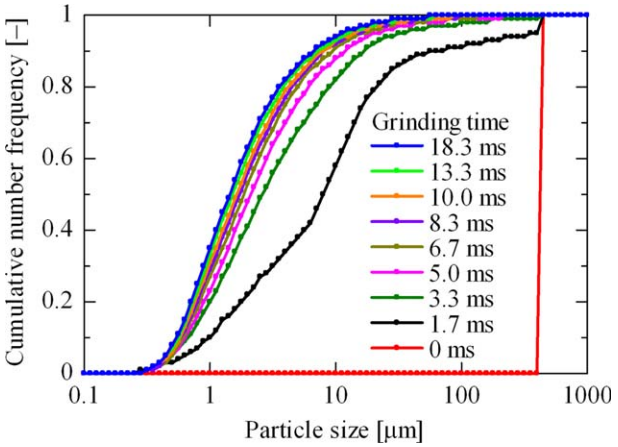

Figure 12. Temporal change in number-based cumulative particle-size distribution in grinding chamber.

[Color figure can be viewed in the online issue, which is available at wileyonlinelibrary.com.]

stage of the grinding, the particle-size distribution of the final ground product was changed because amount of the collected particles was tiny. However, with a further increase in the grinding time, the particle-size distribution reached to constant regardless of the grinding time. Thus, the calculated result at $t = 18.3$ ms was compared to the experimental result.

Figure 16 shows particle-size distributions of the fed material and final ground product to compare the numerical simulation result with the experimental result. In this figure, the circles with the dashed line indicate particle-size distribution of the fed material used in the experiment. The solid line at 500 μm indicates an input value of the particle-size distribution of the fed material for the numerical simulation. The triangles with the dashed line show particle-size distribution of the final ground product collected in the collection pot obtained in the experiment. The other solid line shows the calculated result of particle-size distribution of the final ground product which was also collected in the collection pot. In the final ground products, the calculated mass fraction at the size range larger than 100 μm was lower than the experimental one, whereas the calculated mass fraction at the

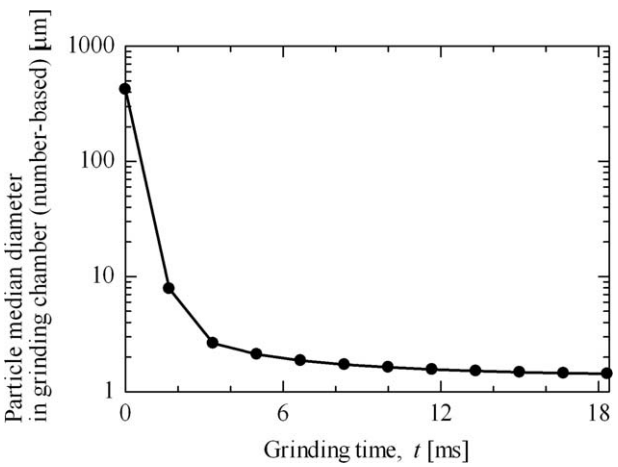

Figure 13. Temporal change in particle median diameter in grinding chamber.

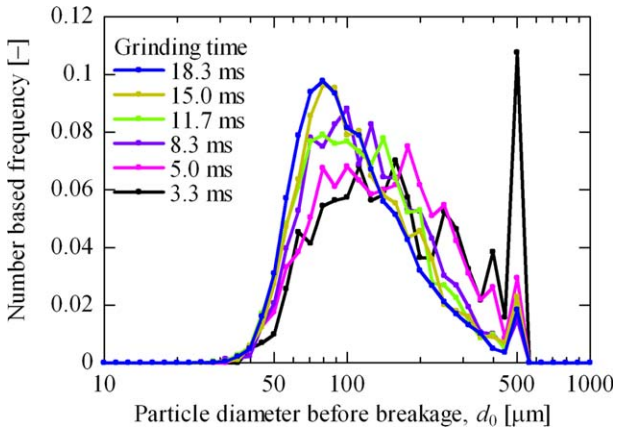

Figure 14. Number-based size distribution of particles before breakage in grinding chamber.

[Color figure can be viewed in the online issue, which is available at wileyonlinelibrary.com.]

size range smaller than 50 μm was higher than the experimental one. This was due to a characteristic of the breakage function (Eq. 11), in which the smaller fragments were more likely to be generated rather than the larger fragments, when the maximum number of the fragments was small. In this study, the maximum number of the fragments was set as 30. This number was preliminary optimized to achieve both better accuracy of calculated fragment size and lower computing cost. Nevertheless, the calculated particle-size distribution of the final ground product showed acceptable agreement with the experimental one. In summary, the prediction of the particle-size distribution of a final ground product in a grinding process can be possible using the proposed numerical simulation method.

Conclusions

A new method to simultaneously simulate the particle motion and its breakage in a dry impact pulverizer was developed. The motion of the particles in the pulverizer was calculated using DPM-CFD coupling model. When the particle impacted against a wall, the impact stress was calculated from Hertz's theory as a function of the impact velocity. At

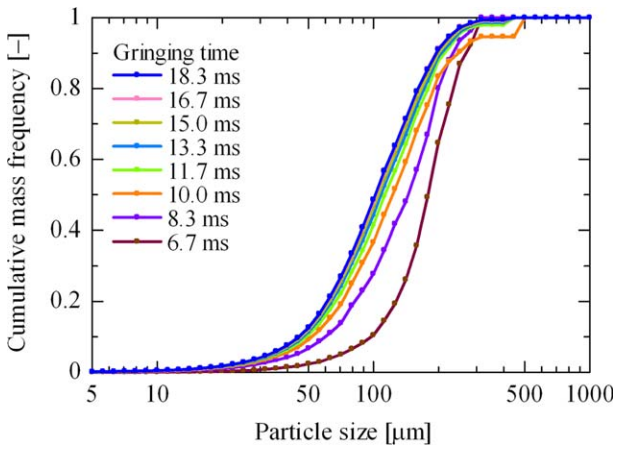

Figure 15. Temporal change in calculated particle-size distribution of final ground product.

[Color figure can be viewed in the online issue, which is available at wileyonlinelibrary.com.]

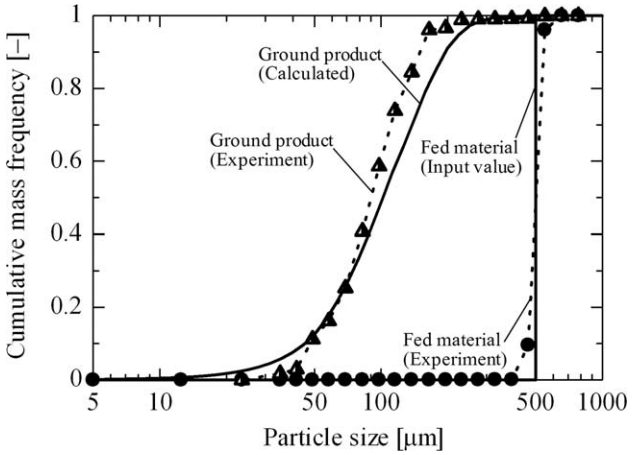

Figure 16. Comparison of calculated particle-size distribution of ground products with experimental one.

the same time, the particle strength was calculated from Griffith's theory. When the impact stress was larger than the particle strength, the particle was broken and replaced with smaller particle, namely fragments. The size distribution of the fragments was obtained from a breakage function. The motion of the fragments was calculated again using the DPM-CFD coupling model. By repeating the above calculations for all particles in the impact pulverizer, the grinding phenomenon could be simulated.

The particle strength which was obtained from a uniaxial compression test could be well-described by Griffith's theory under the assumption that the crack length obeys a log-normal distribution. The size distribution of the fragments which was obtained from an impact breakage test was described by a power-low function. The parameter of the power-low function could be expressed as a function of the impact velocity. The calculated results of particle motion and its breakage behavior showed similar results to that in actual grinding behavior such as a particle-size reduction, increase in number of the particles, and size limitation of the particles which can be broken. The simulation results also exhibited clearly where and how the particles were broken in the grinding chamber. The calculated particle-size distribution of the final ground product showed acceptable agreement with an experimental one. The proposed simulation method enables us to predict a particle-size distribution of a final ground product. This simulation method can assist design of grinding process and optimization of the operating conditions.

Notation

a = parameter in Eq. 6, nondimension
B = volume ratio of fragments, nondimension
C = half-length of crack, m
C_d = coefficient of fluid drag, nondimension
d = particle diameter, m
d_0 = particle diameter before breakage, m
d_i = particle diameter of a fragment, m
d_{min} = minimum particle diameter of fragments, m
E = Young's modulus, Pa
F_B = particle breakage load, N
F_d = fluid drug force, N
F_I = maximum impact load, N
$f(C)$ = crack-length distribution, nondimension
g = gravity acceleration, m/s^2
K_1 = empirical constant, nondimension
K_2 = empirical constant, nondimension
K_3 = empirical constant, nondimension
k = parameter defined by Eq. 4, nondimension
m_p = particle mass, kg
N = number ratio of the fragments, nondimension
Re_p = particle Reynolds number, nondimension
S_c = geometric mean of crack length, nondimension
t = grinding time, s
u = fluid velocity, m/s
u_p = particle velocity, m/s

Greek letters

γ = surface energy, J/m^2
μ = fluid viscosity, Pa s
μ_c = standard deviation of crack length, nondimension
ν = Poisson's ratio, nondimension
ρ_f = fluid density, kg/m^3
ρ_p = particle density, kg/m^3
σ_I = maximum impact stress, Pa
σ_S = tensile strength of particle, Pa

Subscripts

c = crack length
I = impact
p = particle
S = strength

Literature Cited

1. Cleary PW, Sinnott MD, Morrison RD. DEM prediction of particle flows in grinding processes. *Int J Numer Meth Fluids*. 2008;58:319–353.
2. Mori H, Mio H, Kano J, Saito F. Ball mill simulation in wet grinding using a tumbling mill and its correlation to grinding rate. *Powder Technol*. 2004;143–144:230–239.
3. Theuerkauf J, Schwedes J. Theoretical and experimental investigation on particle and fluid motion in stirred media mills. *Powder Technol*. 1999;105:406–412.
4. Bhasker C. Numerical simulation of turbulent flow in complex geometries used in power plants. *Adv Eng Softw*. 2002;33:71–83.
5. Shah KV, Vuthaluru R, Vuthaluru HB. CFD based investigations into optimization of coal pulveriser performance: effect of classifier vane settings. *Fuel Process Technol*. 2009;90:1135–1141.
6. Eskin D, Zhupanska O, Hamey R, Moudgil B, Scarlett B. Microhydrodynamics of stirred media milling. *Powder Technol*. 2005;156:95–102.
7. Chatzilamprou IG, Youds MW, Tierney MJ, Armstrong B. Numerical investigation of a developmental pneumatically fed impact pulveriser. *Appl Math Model*. 2006;30:1180–1195.
8. Takeuchi H, Nakamura H, Iwasaki T, Watano S. Numerical modeling of fluid and particle behaviors in impact pulverizer. *Powder Technol*. 2012;217:148–156.
9. Gers R, Climent E, Legendre D, Anne-Archard D, Frances C. Numerical modelling of grinding in a stirred media mill: hydrodynamics and collision characteristics. *Chem Eng Sci*. 2010;65:2052–2064.
10. Kwan CC, Mio H, Chen YQ, Ding YL, Saito F, Papadopoulos DG, Bentham AC, Ghadiri M. Analysis of the milling rate of pharmaceutical powders using the distinct element method (DEM). *Chem Eng Sci*. 2005;60:1441–1448.
11. Jayasundara CT, Yang RY, Guo BY, Yu AB, Govender I, Mainza A, Westhuizen A, Rubenstein J. CFD-DEM modelling of particle flow in IsaMills-comparison between simulations and PEPT measurements. *Miner Eng*. 2011;24:181–187.
12. Wittel FK, Carmona HA, Kun F, Herrmann HJ. Mechanisms in impact fragmentation. *Int J Fract*. 2008;154:105–117.
13. Tong ZB, Yang RY, Yu AB, Adi S, Chan HK. Numerical modelling of the breakage of loose agglomerates of fine particles. *Powder Technol*. 2009;196:213–221.
14. Vogel L, Peukert W. From single particle impact behavior to modelling of impact mills. *Chem Eng Sci*. 2005;60:5164–5176.
15. Kalman H, Rodnianski V, Mordechai H. A new method to implement comminution functions into DEM simulation of a size reduction system due to particle-wall collisions. *Granul Matter* 2009;11:253–266.
16. Herbst J, Potapov A. Making a discrete grain breakage model practical for comminution process performance simulation. *Powder Technol*. 2004;143–144:144–150.

17. Herbst J, Potapov A, Hambidge G, Rademan J. Modeling of diamond liberation and damage for Debswana kimberlitic ores. *Miner Eng*. 2008;21:766–769.
18. Lichter J, Lim K, Potapov A, Kaja D. New developments in cone crusher performance optimization. *Miner Eng*. 2009;22:613–617.
19. Cleary PW. Recent advances in DEM modelling of tumbling mills. *Miner Eng*. 2001;14:1295–1319.
20. Bruchmüller J, Wachem BGM, Gu S, Luo KH. Modelling discrete fragmentation of brittle particles. *Powder Technol*. 2011;208:731–739.
21. Potapov AV, Campbell CS. Computer simulation of impact induced particle breakage. *Powder Technol*. 1994;81:207–216.
22. Potapov AV, Campbell CS. Computer simulation of shear-induced particle attrition. *Powder Technol*. 1997;94:109–122.
23. Griffith AA. The theory of rupture. In: *Proceedings of the 1st International Congress of Applied Mechanics*. Delft, Nederland: Dutch Technical University, 1924:55–63.
24. Knight CG, Swain MV, Chaudhri MM. Impact of small steel spheres on glass surfaces. *J Mater Sci*. 1977;12:1573–1586.
25. Sahoo R. Review: an investigation of single particle breakage tests for coal handling system of the gladstone port. *Powder Technol*. 2006;161:158–167.
26. Meier M, John E, Wieckhusen D, Wirth W, Peukert W. Generally applicable breakage functions derived from single particle comminution data. *Powder Technol*. 2009;194:33–41.
27. Wu SZ, Chau KT, Yu TX. Crushing and fragmentation of brittle spheres under double impact test. *Powder Technol*. 2004;143–144:41–55.
28. Nikolov S. A performance model for impact crushers. *Miner Eng*. 2002;15:715–721.
29. Bird RB, Stewart WE, Lightfoot EN. Transport phenomena, 2nd ed. New York: John Wiley & Sons, Inc., 2002.
30. Shih TH, Liou WW, Shabbir A, Yang Z, Zhu J. A new k-ε eddy-viscosity model for high Reynolds number turbulent flows-model development and validation. *Comput Fluids*. 1995;24:227–238.
31. Morsi SA, Alexander AJ. An Investigation of particle trajectories in two-phase flow systems. *J Fluid Mech*. 1972;55:193–208.
32. Box GEP, Muller ME. A note on the generation of random normal deviates. *Ann Math Stat*. 1958;29:610–611.
33. Matsumoto M, Nishimura T. Mersenne Twister: a 623-dimensionally equidistributed uniform pseudo-random number generator. *ACM Trans Model Comput Simul*. 1998;8:3–30.
34. Goldsmith W, Lyman PT. The penetration of hard-steel spheres into plane metal surfaces. *J Appl Mech*. 1960;27:17–25.
35. Potapov AV, Campbell CS. Parametric dependence of particle breakage mechanisms. *Powder technol*. 2001;22:164–174.

Manuscript received Sept. 11, 2012, revision received Dec. 17, 2012, and final revision received Mar. 12, 2013.